Silica-supported ionic liquids for heat powered sorption desalination

Silica-supported ionic liquids for heat powered sorption desalination

Ahmed Askalany[a,b], Christopher Olkis[b], Emilia Bramanti[c], Dmitry Lapshin[b], Luigi Calabrese[d], Edoardo Proverbio[d], Angelo Freni[c], Giulio Santori[b].*

[a] Mechanical Engineering Department, Faculty of Industrial Education, Sohag University, Sohag, 82524, Egypt

[b] The University of Edinburgh, School of Engineering, Institute for Materials and Processes, Sanderson Building, The King's Buildings, Robert Stevenson Road, Edinburgh, Scotland, EH9 3FB, UK

[c] Consiglio Nazionale delle Ricerche, Istituto di Chimica dei Composti Organometallici (CNR-ICCOM) Via G. Moruzzi, 1, Pisa, 56124, Italy

[d] Department of Engineering, University of Messina, Messina, 98122, Italy

ORCID iDs of the authors
Ahmed Askalany: 0000-0003-0675-5917
Christopher Olkis: 0000-0002-1466-919X
Emilia Bramanti: 0000-0001-8478-7370
Dmitry Lapshin: 0000-0001-8507-9042
Luigi Calabrese: 0000-0002-2923-7664
Edoardo Proverbio: 0000-0002-6679-7214
Angelo Freni: 0000-0003-2537-6365
Giulio Santori: 0000-0003-2156-6647

KEYWORDS: Supported ionic liquid, desalination, water, sorption, ionogel.

ABSTRACT: This work investigates the application of novel sorption materials to heat-powered desalination systems. Two ionic liquids 1-ethyl-3-methylimidazolium acetate (Emim-Ac) and 1-ethyl-3-methylimidazolium methanesulfonate (Emim-Oms) ionic liquids were impregnated in two silica supports, namely Syloid AL-1FP and Syloid 72FP. Emim-Ac and Emim-Oms composite sorbents have been compared on morphology, water vapor sorption equilibrium and heat of sorption. Fourier-transform infrared spectroscopy shows the ionic liquid partly organises on the silica surface. When used in a sorption desalination process powered by low grade heat at 60°C, these composites have exceptionally high theoretical working capacities ranging from 1 to 1.7 $g_{water}\ g_{sorbent}^{-1}$. Experimental tests on a lab scale desalinator show that Emim-Ac/Syloid 72FP in real operating conditions can produce 25 $kg_{water}\ kg_{sorbent}^{-1}\ day^{-1}$. To date, this yield is 2.5 times higher than the best achieved with silica gel.

1. Introduction

The development of nanoporous materials for adsorption heat transformation (AHT) has increased in the last decades due to the capability of the AHT process to convert low-grade thermal energy into diverse useful effects such as cooling, [1,2] water purification, [3] atmospheric water harvesting [4], electricity generation [5] and long term thermal energy storage. [6] The AHT process can be applied to water purification as schematized in **Figure 1** and a more extensive description of the application can be found elsewhere. [7]

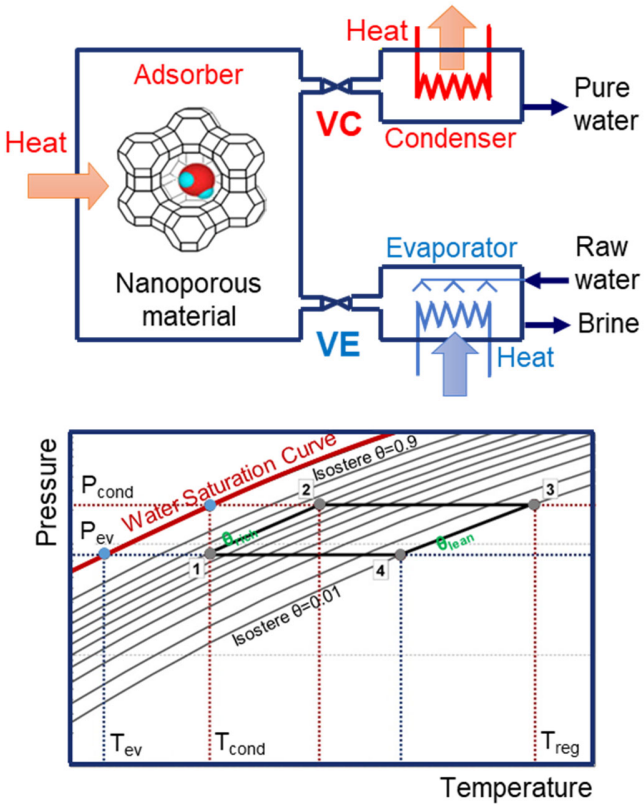

Figure 1. The scheme of a single bed adsorption desalination process (top). It operates by following two steps. Step 1 (desorption, from state 1 to 3): Valve VC is open. The sorption material has already high water uptake (isostere Θ_{rich}) and is heated in the adsorber (regeneration). After an initial heating at constant isostere (from state 1 to state 2), the water vapor released from the adsorber is condensed at ambient temperature as pure water in the condenser (from state 2 to state 3). Step 2 (adsorption, from state 3 to state 1): Valve VE connecting adsorber and evaporator is open. Valve VC connecting adsorber and condenser is closed. Heat at ambient temperature is provided to the evaporator while the adsorber is kept at ambient temperature. After an initial cooling at constant isostere (from state 3 to state 4), water evaporates and is captured in the sorption material (previously regenerated by heating at isostere Θ_{lean}) until state 1. Valve VE is closed. By alternating the operation of the two beds (while one bed is in Step 1 a second bed is in Step 2) the process is made continuous. The process follows a thermodynamic cycle (bottom) defined on three temperatures: evaporation temperature (T_{ev}), condensing temperature (T_{cond}) and regeneration temperature (T_{reg}). In AHT desalinators evaporating, condensing and ambient temperature are close ($T_{ev} \sim T_{cond} \sim T_{amb}$) while T_{reg} can be from renewable or waste heat sources and ranges from 40°C to 70°C.

Adsorption desalination and membrane distillation are the only technological options available for desalination with low-grade heat at temperature <70°C. A comparison on primary energy consumption between adsorption desalination and membrane distillation

(**Figure 2**) shows that membrane distillation is available in many different versions and can span a wide range of performance. Membrane distillation has benefitted of large development efforts that led to commercial devices [8,9] and is currently more mature than adsorption desalination. Nevertheless, the exergy efficiency of adsorption desalination laboratory prototypes is competitive even with the best membrane distillation systems.

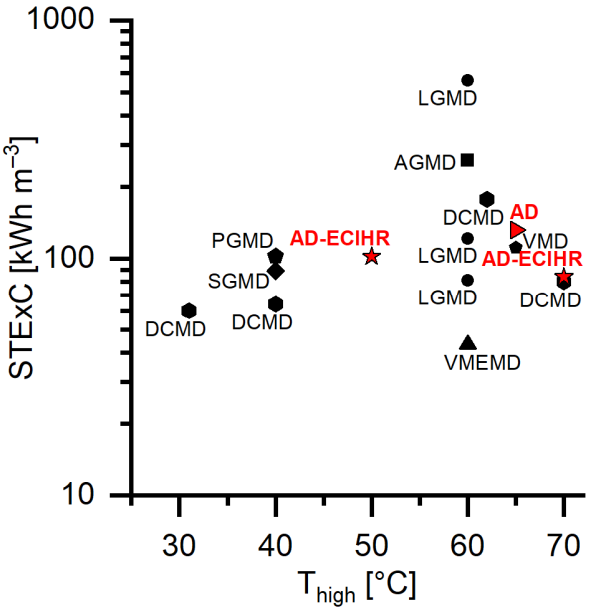

Figure 2. Comparison between adsorption desalination (AD, red symbols) and membrane distillation (MD, black symbols) on the basis of the temperature level of the heat source (T_{high}) and the Specific Thermal Exergy Consumption (STExC). LGMD: Liquid Gap Membrane Distillation (commercial unit) [8]; AGMD: Air Gap Membrane Distillation (commercial unit) [8]; PGMD: Permeate Gap Membrane Distillation (laboratory unit) [10]; SGMD: Sweeping Gas Membrane Distillation (laboratory unit) [10]; DCMD: Direct Contact Membrane Distillation (laboratory units) [9–11]; VMD: Vacuum Membrane Distillation (laboratory unit) [12]; VMEMD: Vacuum Multi Effect Membrane Distillation (commercial unit) [8]; AD: Adsorption Desalination (laboratory unit using silica gel) [13]; AD-ECIHR: Adsorption Desalination Evaporator/Condenser Heat Recovery (laboratory unit using silica gel) [14].

AHT devices are in practice not ready-to-market yet. The first shortfall comes from the low working capacities of the nanoporous materials used so far. The working capacity is defined as the difference in the specific amount of water sorbed [$g_{water}g_{sorbent}^{-1}$] in the

sorption state (state 1 in Figure 1) and desorption state (state 3 in Figure 1) of the thermodynamic cycle. The most promising sorption materials for AHTs are called selective water sorbents (SWSs). [15] These materials are two-component systems consisting of an inorganic salt in a mesoporous silica gel matrix. Sorption equilibrium of SWSs can be tuned by changing the porous structure of the silica gels, salt type, amount of salt loaded in the host nanopores and synthesis conditions. [16] Among the SWSs, $CaCl_2$–mesoporous silica gel [17] and LiBr–mesoporous silica gel [18] composites have unrivalled performance for heat transformation. However, such sorbents have been specifically developed for adsorption cooling purpose and do not show suitable working capacity for desalination. In fact, common commercial microporous silica gel is still the benchmarking material for desalination. [19] An early study has demonstrated that the replacement of macroporous silica gel with aerogels and xerogels results in materials such as the composite $CaCl_2$–xerogel that have exceptional equilibrium features for sorption desalination, improving the working capacity at the desalination operating conditions up to values ~1 $g_{water}g_{sorbent}^{-1}$. [20] Unfortunately, this investigation has been focused only on equilibrium measurements, lacking of the tests needed for the actual utilization of the material in real devices. Crystalline nanoporous materials have been also explored as materials for water-sorptive applications. [21,22] Among these, AQSOA-FAM-Z02, a chabazite type zeolite, has been initially proposed for desalination as an alternative to the benchmark amorphous silica gel [23]. Although its working capacity (~0.27 $g_{water}g_{sorbent}^{-1}$) [5] is attractive, it is still limited and below $CaCl_2$–xerogel. Different metal−organic frameworks (MOFs) such as MIL-101(Cr), aluminium fumarate and CPO-27(Ni) have been also investigated for desalination processes, the latter showing a working capacity of

~0.32$g_{water}g_{sorbent}^{-1}$. [24] This is higher than AQSOA-FAM-Z02 but it can only be achieved when regeneration heat is available at temperatures >90°C. High production cost and low stability upon repeated water sorption cycles are other possible issues limiting the practical use of MOFs. In addition to physisorption in nanoporous materials, many hydrophilic ionic liquids have been investigated as process fluids for thermally-driven technologies. [25] In particular, 1-ethyl-3-methylimidazolium methanesulfonate ionic liquid has shown ~0.77$g_{water}g_{ionic\ liquid}^{-1}$ working capacity in desalination. [26] The drawback of ionic liquid sorbents is their need for multiple components and their corrosive character interwoven to their hydrophilicity. This limits their practical use.

In this work, we have developed a novel silica-supported ionic liquid composite material for water sorption exceeding the performance of $CaCl_2$–xerogel. Two silica support materials (Syloid AL-1FP or Syloid 72FP) are impregnated with two different hydrophilic ionic liquids (1-ethyl-3-methylimidazolium acetate, Emim-Ac or 1-ethyl-3-methylimidazolium methanesulfonate, Emim-Oms). Emim-Ac composite sorbents have been compared to Emim-Oms composites. The morphology of the ionic liquids adsorbed onto silica has been investigated by SEM imaging and the interactions between material components studied by infrared spectroscopy. The measurement of the equilibrium properties have allowed to assess the maximum theoretically achievable working capacity and select the best composite that has been tested in a real sorption desalination device.

2. Materials and Methods

Samples preparation. 1-ethyl-3-methylimidazolium methanesulfonate (Emim-Oms) and 1-Ethyl-3-methylimidazolium acetate (Emim-Ac) ionic liquids with a purity ≥95.0% were purchased from Sigma Aldrich. Syloid AL-1FP Silica and Syloid 72FP Silica were obtained from Grace. Composite materials were prepared by means of incipient wetness impregnation method. [16] Syloid silica was dried for 12 hours at 120ºC before mixing with an aqueous solution of ionic liquid of 1:1 ratio on mass basis. After reaching homogeneity by magnetic stirring, water was gently evaporated from the solution at 80ºC. 60wt% concentration of ionic liquid was attained for all the samples.

Scanning Electron Microscopy. Morphology of all batches was evaluated by dual beam scanning electron microscope (Zeiss Crossbeam 540) by using FEG probe @2KV in high-resolution configuration, secondary electrons image by using an Inlens detector.

Fourier Transform Infrared Spectroscopy. Attenuated total reflectance (ATR) -FTIR spectra were recorded by using a Perkin-Elmer Spectrum One FTIR spectrophotometer, equipped with a universal ATR accessory (diamond crystal) and TGS detector. For each sample, 32 interferograms were recorded in order to obtain a suitable S/N ratio, averaged and Fourier-transformed to produce a spectrum with a nominal resolution of 4 cm^{-1} in the 600-4000 cm^{-1} range. The background was preliminarily recorded on the clean diamond crystal. Spectrum software (Perkin-Elmer) was employed to run and process the FTIR spectra. [27–29]

Thermogravimetric analysis. Thermogravimetric (TG) analyses were carried out under nitrogen atmosphere using a Seiko EXSTAR 7200 TG/DTA instrument. TG curves were

collected on samples of 5-8 mg in the temperature range from 30°C to 900°C (N_2 flow =200 ml min^{-1}) with a heating rate of 10°C min^{-1}.

Sorption gravimetric microbalance. Water sorption isotherms of silica-supported ionic liquids were measured using a Gravimetric Vapour Sorption Analyser AQUADYNE DVS (Quantachrome Instruments). This device has ultrasensitive electronic microbalances with an accuracy of ±1.0 μg working in range of 15-60°C. Measurement at 25°C were performed on for two pure silica supports (Syloid AL-1FP and Syloid 72FP) and 4 composites Emim-Oms/Syloid AL-1FP, Emim-Oms/Syloid 72FP, Emim-Ac/Syloid AL-1FP and Emim-Ac/Syloid 72FP. Water vapor sorption of Emim-Ac/Syloid AL-1FP and Emim-Ac/Syloid 72FP was also measured in an extended temperature range between 25 and 55°C.

Adsorption desalinator. 66g of Emim-Ac/Syloid 72FP powder were integrated within the aluminium heat exchanger of a lab scale adsorption desalination apparatus resulting in an ionogel monolithic structure. The adsorption desalinator has been detailed elsewhere.[30,31] The small-scale design of the test-rig enables the testing of small samples (25g-200g) of adsorption materials. The test rig was used in one-bed mode.

3. Results and discussion

3.1. Material characterization

Table 1 reports the physical features of the two silica supports investigated in this work. Syloid FP silica are silica gels with a particularly high density of surface silanol groups (≡Si–OH), commercially used as moisture controllers in pharmaceutical and personal care products.

Table 1. Physical features of the silica supports.

Property	Syloid AL-1FP	Syloid 72FP
Avarage particle size (μm)	6.5–8.1 [32]	4.6–5.8 [32]
Bulk density (g l^{-1})	566 [32]	112 [32]
Average Pore Volume (cm^3 g^{-1})	0.23–0.40 [33,34]	1.2 [32,34]
Average Pore Diameter (Å)	26–30 [33,34]	100–150 [34–36]
BET Surface Area (m^2 g^{-1})	605–740 [33,34]	340–405 [34–36]

The two silicas were impregnated with 1-ethyl-3-methylimidazolium methanesulfonate (Emim-Oms) and 1-Ethyl-3-methylimidazolium acetate (Emim-Ac) ionic liquids. These two ionic liquids were selected for their high affinity with water after the analysis of their vapor liquid equilibrium data.[37–39] Previous investigations have shown that 60wt% impregnation of ionic liquid in the silica support is the maximal achievable impregnation and also the amount enabling the best theoretical desalination performance. [26,40] When nano-confined, ionic liquids can form ordered multi-layers that functionalise the supporting surface depending on its charge. [26,41] Ordered ionic liquids have shown working capacity [$g_{water}g_{ionic\ liquid}^{-1}$] higher than disordered bulk-state ionic liquids. [26] Therefore the self-organisation of the ionic liquid on the surface of a charged support is beneficial to boost the temperature-swing water sorption equilibrium properties of the ionic liquid. Usually this special behaviour shows at impregnations below 10wt%. In this range of low impregnation, the interfacial properties of the ionic liquid are dominant over the bulk properties. [42]

Impregnations below 10wt% benefit from the interfacial properties of the ordered ionic liquids that are often advantageous for temperature swing sorption processes. [42] Nevertheless, to maximize the practical performance of a desalination device it is beneficial to load the porous support material to completely fill the pores and the external surface of the particles. This allows higher working capacities [$g_{water}g_{sorbent}^{-1}$] than what can be achieved at low impregnation. **Figure 3** shows SEM images of the pristine and impregnated Syloid 72FP silica carrier used in this study. The surface morphology of pure Syloid 72FP (sample A) is characterized by agglomerates without a regular structure with an average grain size in the range 1-5 μm (Figure 3a). At higher magnification (Figure 3b and Figure 3c), the extremely fine microstructure is clearly visible. The microstructure is responsible for the large surface area in Table 1 with a highly developed network of mesopores. SEM imaging of Syloid 72FP impregnated at 60wt% with Emim-Ac (sample B) shows that the superficial channels are still visible, although they are partially obstructed by the ionic liquid (Figure 3d-f). This is a consequence of the ionic liquid that unevenly occupies the internal porosity of the amorphous silica. The impregnation with 60wt% Emim-Oms shows similar behavior (Figure 3g-i): the pore volume is filled with ionic liquid although the pores are only partially filled in some cases. Ionic liquid is present also on the external surface of the particles.

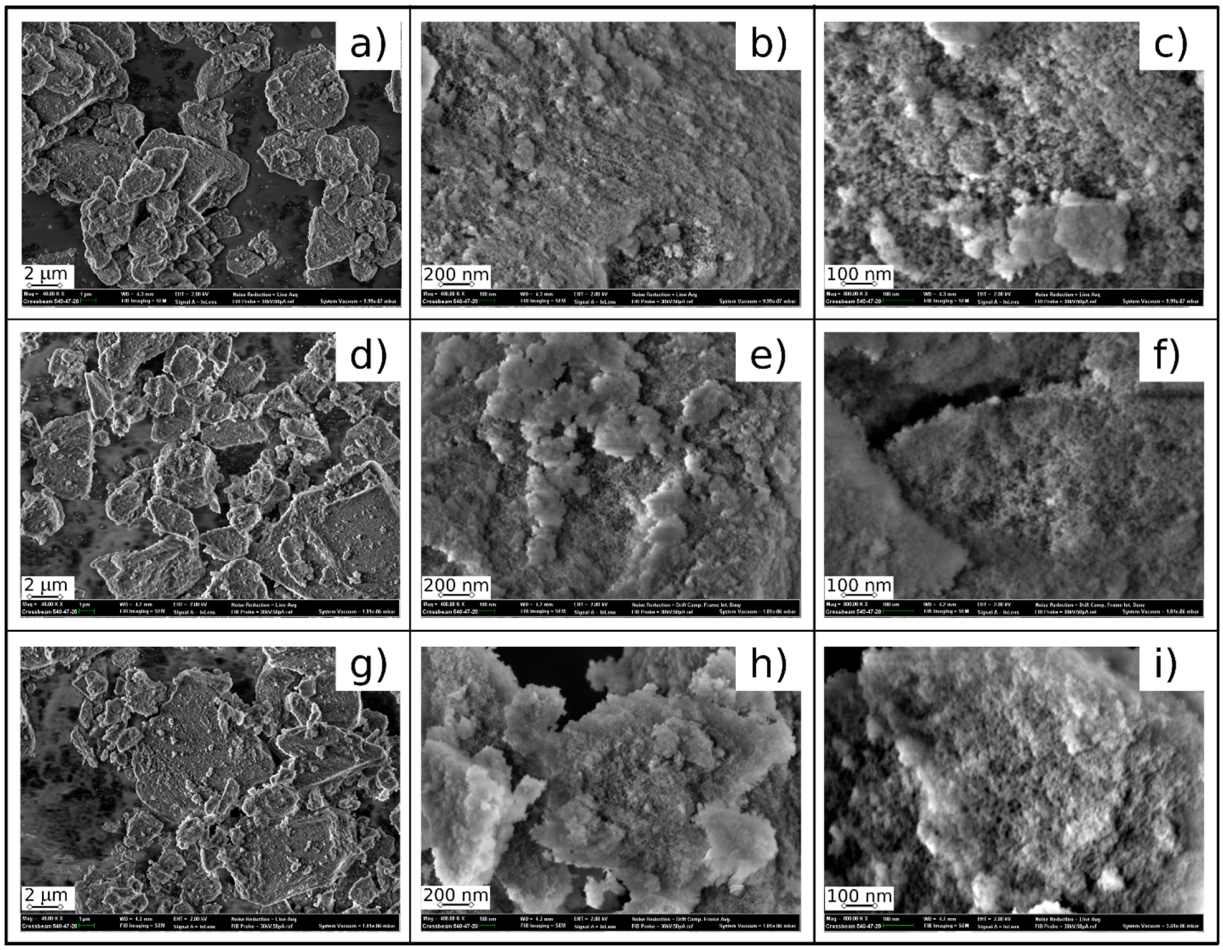

Figure 3. SEM images at different magnifications (low - 40,000x, medium – 400,000x, high – 800,000x) of (a-b-c) sample A - Syloid 72FP, (d-e-f) sample B - 60wt% Emim-Ac/Syloid 72FP, (g-h-i) sample C - 60wt% Emim-Oms/Syloid 72FP.

Attenuated total reflectance (ATR) -FTIR spectroscopy was used to monitor the presence of Emim-Ac in Syloid 72 FP and determine its interactions with the silica matrix. The ATR-FTIR spectra of pristine Emim-Ac, Syloid 72FP and 60wt% Emim-Ac/Syloid 72FP composite are shown in **Figure 4** in the 4000–600, 1750–1275 and 1275–1000 cm^{-1} range, respectively.

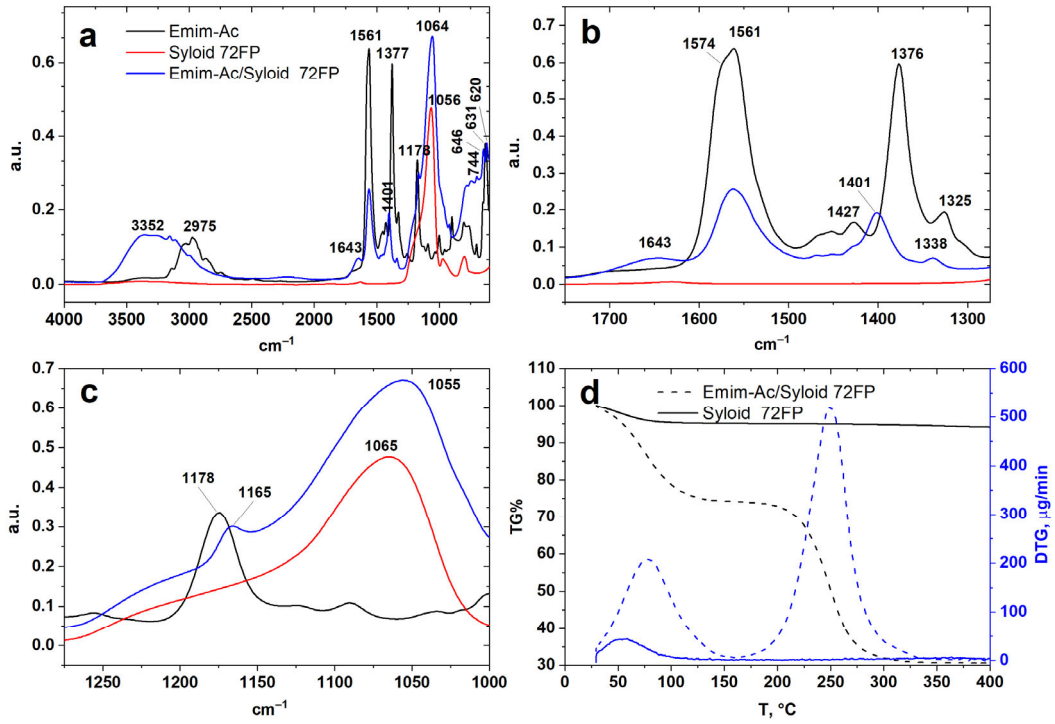

Figure 4. (a) ATR-FTIR spectra of Emim-Ac ionic liquid, Syloid 72FP and 60wt% Emim-Ac/Syloid 72FP composite in the (a) 4000–600 cm^{-1}, (b) 1750–1275 cm^{-1} and (c) 1275–1000 cm^{-1} range. (d) Thermogravimetric analysis of Syloid 72FP and 60wt% Emim-Ac/Syloid 72FP composite in the 20–400°C temperature range.

Syloid 72FP FTIR spectrum is characterized by a broad intense Si–O absorption band at 1250–1000 cm^{-1}. [43] In the FTIR spectrum of pristine Emim-Ac (Figure 4a, 4b and 4c, black line) the spectral bands above 3000 cm^{-1} corresponds to the C–H vibrational modes of the imidazolium ring. The bands between 2900 and 2800 cm^{-1} are due to the aliphatic asymmetric (C–H) stretching vibrations, symmetric and asymmetric stretching modes of CH_2 and CH_3 respectively. The complex band at 1561 cm^{-1} with a shoulder at 1574 cm^{-1} is due to the antisymmetric C=O stretching of acetate anion interacting with the imidazolium ring of the cation. In this specific case no significant amounts of physisorbed water is present in pristine Emim-Ac, considering the absence of OH stretching band around 3400 cm^{-1} and OH bending band at 1650 cm^{-1} of water.

The IR vibration bands at 1376 cm^{-1} and 1178 cm^{-1}, 1000 cm^{-1} are assigned to symmetric stretching of the C=O bond of the anion and to C–C, C–N asymmetric stretching and C–H bending vibrations of imidazolium ring respectively. The bands present at 1120–1000 cm^{-1} and 940–890 cm^{-1} are due to C–O stretching and out-of-plane deformation vibrations of the acetate anion. [44] The band at 630 cm^{-1} is assigned to alkane C–H bending vibrations. The broad spectral bands at 500–600 cm^{-1} is due to the organic metal complex formation. [45]

Once loaded into the Syloid 72FP matrix, Emim-Ac strongly interacts with the silica matrix and water eventually physisorbed. Since the average micropore width is 1 nm and the surface of silica particles is negatively charged through silanol groups, a highly ordered structure of Emim-Ac is expected. The interaction of silica phase with Emim-Ac is confirmed by the significant shifts of Si–O stretching band from 1065 of Syloid to 1055 cm^{-1} of Emim-Ac/Syloid 72FP likely due to the formation of hydrogen bonds between the Si–OH groups and the ionic liquid. Moreover, peaks associated with the vibrations of the acetate anion at 1376 cm^{-1} and the second derivative components at 1348 cm^{-1}, 1324 cm^{-1}, 927 cm^{-1}, and 898 cm^{-1} shifted towards 1401 cm^{-1}, 1360 cm^{-1}, 1338 cm^{-1}, 944 cm^{-1}, and 919 cm^{-1} upon impregnation of the ionic liquid in the porous silica. The peaks at 1178 cm^{-1} and 1000 cm^{-1} of the imidazolium cation shift towards 1165 cm^{-1} and 985 cm^{-1} for the composite. These observations confirm that the imidazolium ring of the cation interacts with the negatively charged surface. Moreover, significant changes in the molecular structure of the anion indicate that it stays in the center of a micropore, surrounded by cations.

FTIR analysis shows that water adsorbs in porous structure upon impregnation of silica with the ionic liquid (Figure 4a and 4b, blue line). The broad bands around 3300 cm^{-1} and 1643 cm^{-1} observed for Emim-Ac/Syloid 72FP composite are due to the OH stretching and OH bending

modes, respectively, of water molecules present in pores of the impregnated material. The described above changes in the frequency of C=O asymmetric (1561–1566 cm^{-1}) and symmetric (1376–1401 cm^{-1}) stretching modes of the acetate ion in Emim-Ac and Emim-Ac/Syloid 72FP composite are also affected by the interaction of the anion with physisorbed water. The presence of water molecules may lead to the formation of a solvation shell around the acetate anion, leading to weaker interaction between ions.

ATR-FTIR spectra of Emim-Ac/Syloid 72FP composite after utilization in the desalination device for 500 cycles (temperature cycle 20-60°C; 50-95% RH) did not evidenced detectable alterations of the material (not shown for clarity) demonstrating its hydrothermal stability.

In the thermogravimetric analysis (TGA) the pristine Emim-Ac has shown one step thermal degradation starting at 207°C. [46] In Figure 4d, TGA of the pristine Syloid 72FP shows ~3% loss of sorbed water around 55°C. The 60wt% Emim-Ac/Syloid 72FP composite has two degradation steps at 77.1°C (25.3% weight loss) due to water desorption and at 248.7°C (43.4% weight loss) due to Emim-Ac, with 30.3% residual weight of the Syloid 72FP. This confirms the impregnation of Syloid with 59 ± 2wt% Emim-Ac and the stability of the material in the operating conditions of the desalination cycle.

3.2. Water vapor sorption

Figure 5 shows the gravimetric measurements of water sorption equilibrium isotherms of pure Syloid AL-1FP, Syloid 72FP and silica-supported ionic liquids impregnated at 60wt% Emim-Oms/Syloid AL-1FP, Emim-Oms/Syloid 72FP, Emim-Ac/Syloid AL-1FP and Emim-Ac/Syloid 72FP. The equilibrium isotherms are essential to the calculation of the desalination cycle in Figure 1 and accordingly to rank the material combinations on working capacity. The theoretical working capacity was calculated from the individual characteristic curves for all the preparations. [47] Emim-Ac/Syloid 72FP has the highest water vapor uptake while no significant differences were observed among Emim-Oms/Syloid AL-1FP, Emim-Oms/Syloid 72FP and Emim-Ac/Syloid AL-1FP. Table 2 shows a comparison of the results and their analysis through the two level full factorial design, that is a known statistical technique. [48] In this case, the full factorial design allows to separate and quantify the effect on the working capacity of: i) the type of support material; ii) the type of ionic liquid and; iii) the presence of any eventual interaction between ionic liquid and silica which would be beneficial or detrimental to the desalination performance.

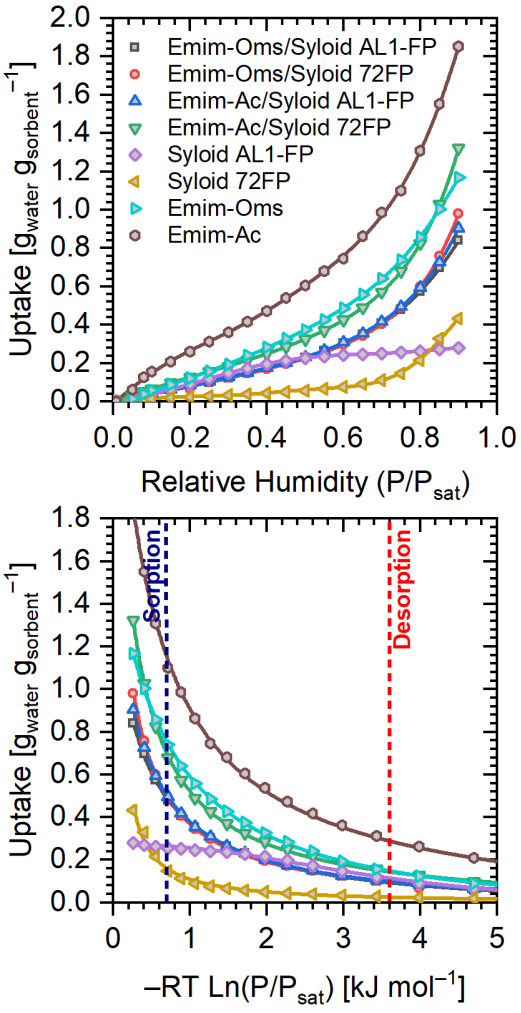

Figure 5. Experimental adsorption isotherms at 25°C (top) from the gravimetric vapor sorption microbalance and characteristic curves (bottom) of the materials under investigation. All composite materials are impregnated with 60wt% of ionic liquid. The dashed straight lines mark the value of $-RTln(P/P_{sat})$ at the adsorption and desorption conditions by considering a thermodynamic sorption desalination cycle with $T_{cond} = T_{sorpt} =$ 25°C; $T_{ev} =$ 20°C and $T_{reg} =$ 50°C.

Table 2. Full factorial analysis on different combinations of ionic liquid and silica.

Silica	Ionic liquid	Working capacity* [$g_{water}\ g_{sorbent}^{-1}$]	Effect* [$g_{water}\ g_{sorbent}^{-1}$]
Syloid AL1-FP	Emim-Oms	0.361	0.395 (mean)
Syloid 72FP	Emim-Oms	0.351	0.056 (Silica)
Syloid AL1-FP	Emim-Ac	0.373	0.078 (Ionic liquid)
Syloid 72FP	Emim-Ac	0.495	0.066 (interaction Silica/Ionic liquid)

Note: *Effect of the change of each single variable (type of silica, type of ionic liquid) or binary interaction between variables (interaction Silica/Ionic Liquid) on the working capacity.

Water sorption curves shown in Figure 5 demonstrate that the type of ionic liquid influences the working capacity more than other factors, increasing it by 0.078 g_{water} $g_{sorbent}^{-1}$ upon changing from OMs to Ac anion. This result agrees with other studies in which the Ac anion has been proved to have larger affinity with water than OMs anion. [37] Moreover, tailored silica-support properties can contribute to the increase of the working capacity. In this specific case, the working capacity increased by 0.056 g_{water} $g_{sorbent}^{-1}$ upon moving from Syloid AL1-FP to Syloid 72 FP. By matching the results in Table 2 with the silica features in Table 1, the combination of support having large pore volume with ionic liquids having high water affinity results in composites with optimal working capacities. **Figure 6** shows a more detailed analysis of the water vapour isotherms at 25.0°C, 34.7°C, 44.4°C and 54.2°C and characteristic curves of Emim-Ac/Syloid 72FP and Emim-Oms/Syloid 72FP composites impregnated with 60wt% ionic liquid. Solid lines are from the Dubinin-Astakhov (DA) isotherm regressions. [49]

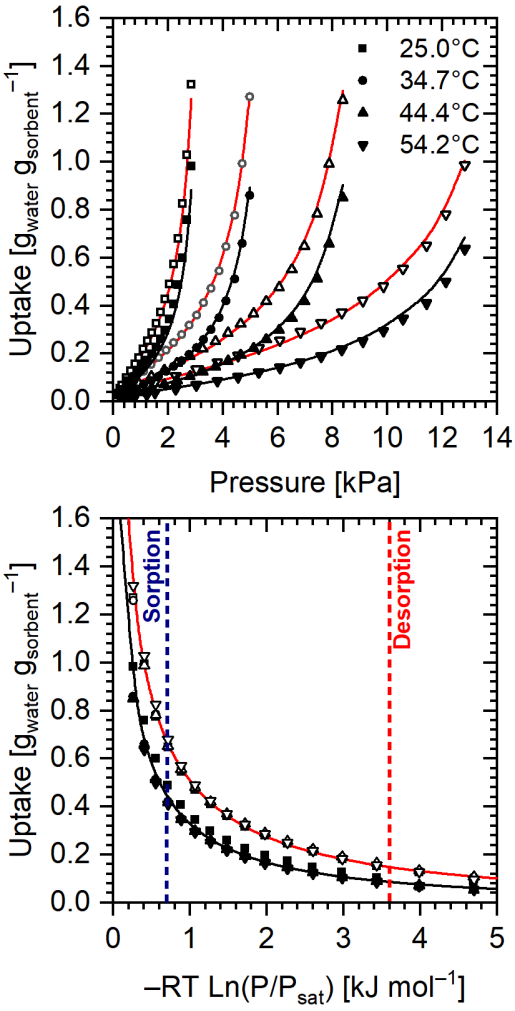

Figure 6. Experimental adsorption isotherms at 25.0°C, 34.7°C, 44.4°C and 54.2°C (top) from the gravimetric vapor sorption microbalance and characteristic curves (bottom) of Emim-Ac/Syloid 72FP (open symbols) and Emim-Oms/Syloid 72FP (filled symbols). All composite materials contain 60wt% ionic liquid. Solid lines are from the Dubinin-Astakhov isotherm regressions. The dashed straight lines in the bottom graph mark the same sorption and desorption conditions of Figure 5.

The DA isotherm appropriately fits the experimental data and corresponds to the expression:

$$w = \frac{v_0}{v_a} exp\left\{-\left(\frac{RT}{E} ln\left(\frac{P_{sat}}{P}\right)\right)^n\right\} \quad (1)$$

where w is the uptake [$g_{water}\ g_{sorbent}^{-1}$], v_0 the water volumetric saturation capacity [$cm_{water}^3\ g_{sorbent}^{-1}$], R the universal gas constant [kJ $kmol^{-1}\ K^{-1}$], E the characteristic energy [kJ $kmol^{-1}$], P the pressure [kPa], P_{sat} the water saturation pressure [kPa] at the equilibrium temperature and n is the isotherm regression constant. The specific volume of the adsorbed phase v_a [$cm_{water}^3\ g_{water}^{-1}$] is estimated by the rectilinear diameters law: [50]

$$v_a = \left(BT - \frac{1}{V_{sat}}\right)^{-1} \quad (2)$$

where v_{sat} is the water saturated vapour specific volume [$cm^3\ g^{-1}$] at the equilibrium temperature and B [kg $m^{-3}\ K^{-1}$] is the fitting constant. The values of the fitting parameters of the DA isotherm are reported in Table 3.

Table 3. Fitting parameters of the DA isotherm for the composites Emim-Oms/Syloid 72FP Emin-Ac/Syloid 72FP loaded with 60wt% ionic liquid.

Parameter	Unit	Emim-Oms/Syloid 72FP	Emin-Ac/Syloid 72FP
v_0	$cm_{water}^3\ g_{sorbent}^{-1}$	38.78	37.06
E	J mol^{-1}	12.80	16.03
n	--	0.27	0.27
B	kg $m^{-3}\ K^{-1}$	0.74	0.90
AAD*	$g_{water}\ g_{sorbent}^{-1}$	0.020	0.016

*average absolute deviation between experimental and calculated uptakes

In Figure 5, the experimental data at different temperatures collapse in a single temperature-independent characteristic curve. This is an interesting feature of this type of materials because it enables the measurement of a single isotherm instead of a full set to provide enough information for quantifying the working capacity of a material in a sorption desalination cycle.

A second fundamental characteristic of optimal sorption materials is their low energy of desorption. The minimum thermodynamic desorption energy coincides with the latent

heat of the specific fluid adsorbed (water in this case). Every additional interaction between water and sorbent increases the amount of binding energy, resulting in energy of desorption larger than the latent heat. The desorption energy depends on the differential sorption enthalpy curve that can be derived from the Clausius-Clapeyron equation by using the sorption isotherm, provided that the isotherm accurately fits the experimental data. For an ideal adsorbed phase the definition of differential sorption enthalpy is:

$$h_{diff} = -\mathrm{RT}^2 \left(\frac{\partial lnP}{\partial T}\right)_{\vartheta} \quad (3)$$

The application of the definition on the DA isotherm results in:

$$h_{diff} = L + E\left[ln\left(\frac{1}{\vartheta}\right)\right]^{\frac{1}{n}} + \frac{ET\alpha}{n}\left[ln\left(\frac{1}{\vartheta}\right)\right]^{\frac{1-n}{n}} \quad (4)$$

where $\theta = (v_a/v_0)$ is the fractional filling, L is the latent heat [kJ kg^{-1}] and α [K^{-1}] is the thermal expansion coefficient of the adsorbed fluid [50] which is:

$$\alpha = v_a\left(B - \frac{\alpha_g}{v_{sat}}\right) \quad (5)$$

where α_g [K^{-1}] is the bulk vapour phase thermal expansion coefficient of water.

Figure 7 shows the trend of the net differential sorption enthalpy of Emim-Oms/Syloid 72FP and Emin-Ac/Syloid 72FP compared with a benchmarking Silica gel for sorption desalination (Siogel). [51] The heat required to regenerate the two composites is similar and by far below that of the benchmarking silica gel. This is a further advantage of the silica-supported materials, which can provide larger working capacities at lower energy consumption. The desorption energy is almost identical to the latent heat of water over a large range of concentrations.

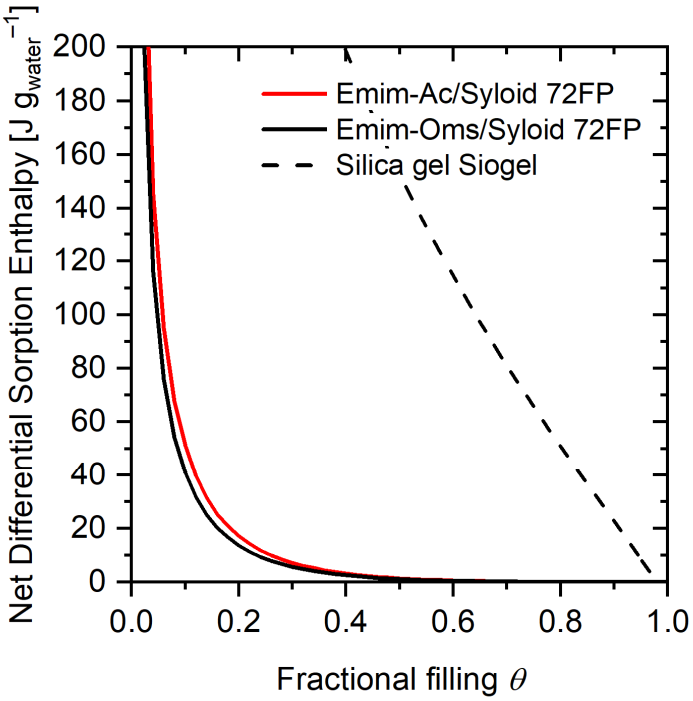

Figure 7. Comparison among the net heat of sorption (difference between differential enthalpy of adsorption and latent heat of water) of Emim-Ac/Syloid 72FP, Emim-Oms/Syloid 72FP and Siogel silica gel used for sorption desalination.

3.3. Application of silica-supported ionic liquids to sorption desalination

Sorption desalination cycles typically work at relative humidity >95%, obtained by operating at close condensation and evaporation temperatures. In all cases, water vapour sorption occurs at room temperature. In these conditions, Emim-Ac/Syloid 72FP and Emim-Oms/Syloid 72FP have high working capacity and require minimal regeneration energy. **Figure 8** shows a theoretical comparison of the working capacity for a desalination cycle of Ionic Liquid/Syloid composites and three advanced, standard materials (SWS-1L, Siogel and CPO27-Ni) assessed from the experimental isotherms.

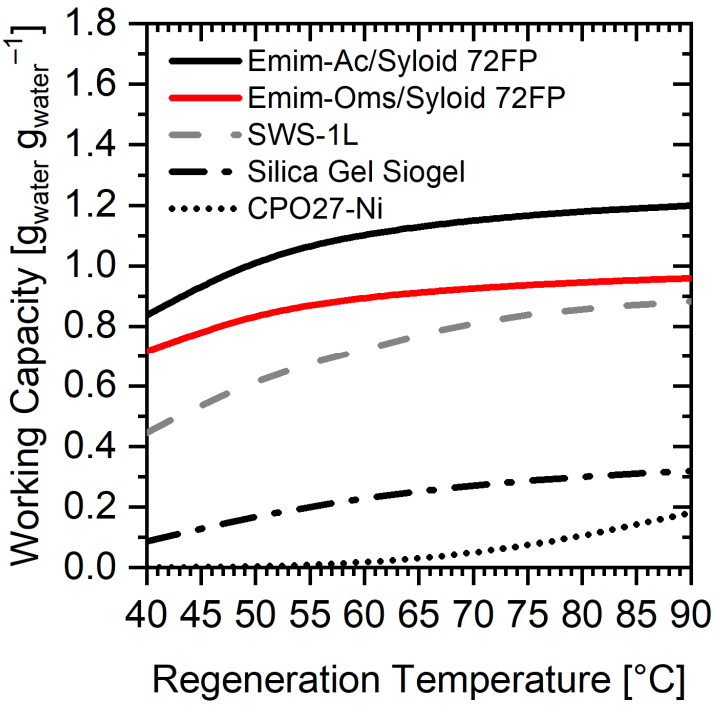

Figure 8. Comparison among the working capacity of different materials for sorption desalination *vs.* regeneration temperatures. Cycle condition are: $T_{cond} = T_{ads} = 30°C$ and $T_{ev} = 25°C$.

These thermodynamic calculations show that the Ionic liquid/Syloid composites have good performance for desalination devices. A lab-scale sorption desalinator has been used to validate the predictions of Figure 8. Further details on the test rig can be found elsewhere.[30,31] Emim-Ac/Syloid 72FP was used at $t_{half\text{-}cycle}$ = 300 s, T_{reg} = 60 °C, inlet temperature of the heat carrier fluid to the condenser and evaporator T_{cond} = 25 °C and T_{ev} = 35 °C, respectively, where the high evaporator inlet temperature ensured that $P_{ev} \approx P_{cond}$. The half cycle time of 300 s was chosen on the basis of preliminary experiments indicating that the best performance can be achieved using short cycle times. The experimental procedure is described in detail elsewhere for silica gel experiments.[31] The experimental apparatus features one evaporator, one condenser and two adsorption beds as given in **Figure 9** and operated in one-bed mode for the experiment presented here.[52]

Each one of the vessels in Figure 9 contains a heat exchangers, which is connected to a thermostatic bath. Cyclic heating and cooling of the adsorption beds powers the process.

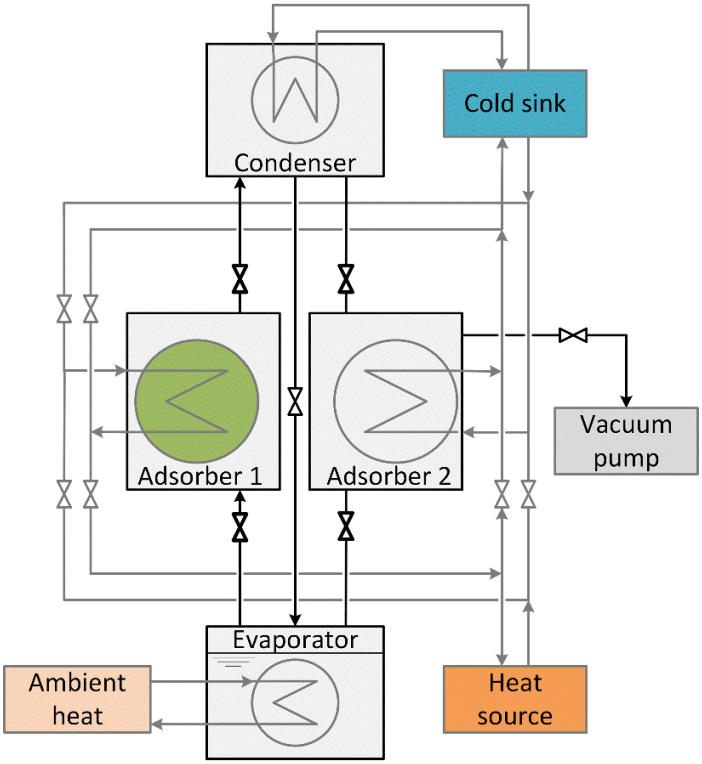

Figure 9. Schematic diagram of the adsorption test rig. The system was used in one bed mode for the experiment presented in this study.

Figure 10 shows the water production based on the utilization of Emim-Ac/Syloid 72FP along with the operating relative humidity of the sorption bed. The sharp peaks in Figure 8 at the beginning of each desorption phase suggest an excellent dynamics thanks to the ionic nature of the composite sorbent. Usually sorption materials do not have good thermal conductivity and this feature makes the cycle times limited by the heat transfer. The time needed to complete half cycle is usually two to five times slower than those reported in Figure 10. [23,53] The experimental working capacity of the material, i.e. 0.26 $g_{water}\ g_{sorbent}^{-1}$, can be further optimized to get the predicted working capacity >1.0 g_{water}

$g_{sorbent}^{-1}$. The material can achieve higher working capacity at 95% relative humidity, which can be reached only at the end of each adsorption. Before this time, the relative humidity remains below 95% because the bed is still cooling from the previous desorption. Moreover, the evaporating water cools the evaporator down, which reduces the evaporation pressure further and makes P_{ev} unstable.

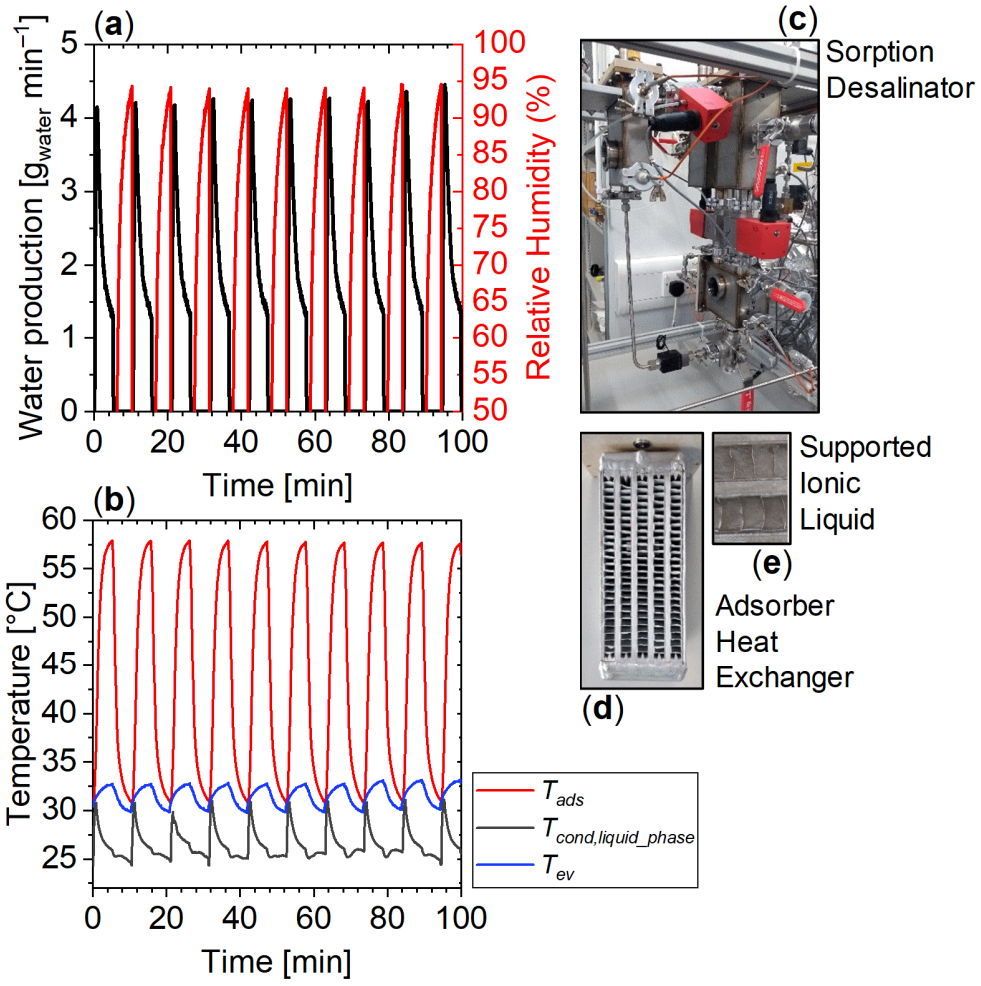

Figure 10. Experimental water production (a) with Emim-Ac/Syloid 72FP regenerated at T_{reg} = 60°C and evolution of the temperatures (b) at the outlet of the adsorber heat exchanger (T_{ads}), of the liquid water in the condenser vessel ($T_{cond,liquid\_phase}$) and of the water vapour in the evaporator (T_{ev}). The value of relative humidity in (a) is calculated from the saturation pressure at T_{ads} and T_{ev}. The sorption desalinator is depicted in (c), a detail of the adsorber heat exchanger is shown in (d) while the supported ionic liquid integrated in the adsorber heat exchanger is shown in (e).

The primary performance indicator to assess the performance of an adsorption desalinator is the Specific Daily Water Production (SDWP [kg_{water} $kg_{sorbent}^{-1}$ day^{-1}]), which illustrates the water throughput of a real system within one day over the course of many cycles:

$$SDWP = N \int_0^{t_{cycle}} \frac{\dot{Q}_{cond}}{L\, M_{AD}} dt \quad (6)$$

where N [-] is the number of cycles performed in a day, L [kJ kg^{-1}] is the latent heat of water, M_{AD} the mass of the adsorption material [kg] and Q_{cond} [kJ s^{-1}] is the condensing power:

$$\dot{Q}_{cond} = \dot{m}_{cond} c_{p,w} (T_{cond,in} - T_{cond,out}) \quad (7)$$

where $\dot{m}$ is the flow rate of cooling water [kg s^{-1}] provided to the condenser heat exchanger, $c_{p,w}$ is the specific heat of the cooling water [kJ kg^{-1} K^{-1}] and $T_{cond,in/out}$ are the temperatures measured at the inlet and outlet flow of the heat exchanger [K].

Due to the fast cycles, the material was able to produce 24.9 kg_{water} $kg_{sorbent}^{-1}$ d^{-1}, which is the highest experimentally validated SDWP for sorption desalination. **Figure 11** shows a comparison of SDWP value for Emim-Ac/Syloid 72FP, CPO27-Ni metal organic framework and Siogel silica gel in analogous operating conditions. [5,24] SDWP of Emim-Ac/Syloid 72FP results 66% higher. Both CPO27-Ni metal organic framework and silica gel require regeneration temperatures >70 °C, while Emim-Ac/Syloid 72P maintains good working capacity also at 60 °C. This allows the utilisation of ultra-low grade heat sources to regenerate this material. Thus, compared with silica gel, Emim-Ac/Syloid 72 shows a 2.5 times higher performance at lower regeneration temperature.

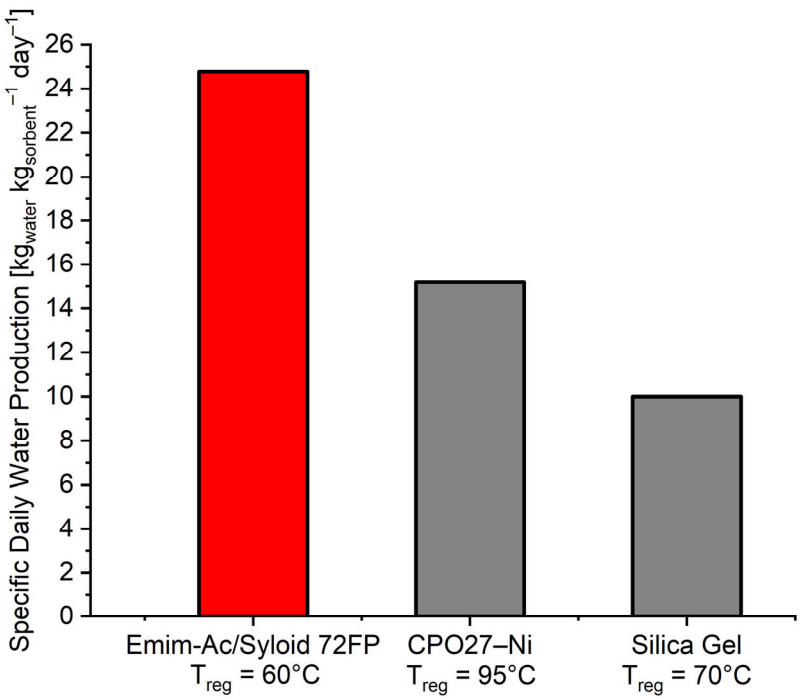

Figure 11. Comparison of the experimental Specific Daily Water Production of Emim-Ac/Syloid 72FP with CPO27-Ni metal organic framework and Siogel silica gel. T_{reg} is the regeneration temperature applied to the sorption bed.

4. Conclusion

Four different composites with 60wt% content of ionic liquid, namely Emim-Oms or Emim-Ac ionic liquids supported onto Syloid AL-1FP and Syloid 72FP silica material have been chemically characterized with SEM imaging and FTIR spectroscopy. The suitability of Emim-Ac/ Syloid 72FP and Emim-Oms/Syloid 72FP for water desalination has been assessed by measuring the equilibrium in the range 25-55°C and regressing the sorption data with a Dubinin-Astakhov model. Emim-Ac/Syloid 72FP has shown the best theoretical performance with a working capacity >1.0 g_{water} $g_{sorbent}^{-1}$. To validate the thermodynamic performance, the material was integrated in a lab-scale adsorption desalination device. [30,31] The experimental tests have shown that in real operating

conditions Emim-Ac/Syloid 72FP can produce 24.9 $kg_{water}\,kg_{sorbent}^{-1}\,d^{-1}$, which is 2.5 times higher than the benchmark silica gel at regeneration temperatures of 60°C. To date, this material shows the highest specific daily water production. Therefore, supported ionic liquid composites have unrivalled properties for heat-powered desalination.

ACKNOWLEDGMENTS

The research leading to these results has received funding from the EPSRC "Micro-scale energy storage for super-efficient wet appliances" project EP/P010954/1.

ABBREVIATIONS

AGMD, Air Gap Membrane Distillation; AD, adsorption desalination; AD-ECIHR, Adsorption Desalination with Evaporator/Condenser Internal Heat Recovery; AHT, adsorption heat transformer; ATR, Attenuated total reflectance; DA, Dubinin-Astakhov; DCMD, Direct Contact Membrane Distillation; Emim-Ac, 1-ethyl-3-methylimidazolium acetate; Emim-Oms, 1-ethyl-3-methylimidazolium methanesulfonate; FTIR, Fourier Transform Infrared Spectroscopy; MD, membrane distillation; LGMD, Liquid Gap Membrane Distillation; MOF, Metal−Organic Frameworks; PGMD, Permeate Gap Membrane Distillation; SDWP, Specific daily water production; SEM, Scanning electron microscopy; SGMD, Sweeping Gas Membrane Distillation; STExC, Specific Thermal Exergy Consumption; TG, thermogravimetric analysis; VMEMD, Vacuum Multi Effect Membrane Distillation; VMD, Vacuum Membrane Distillation.

AUTHOR INFORMATION

Corresponding Author

* Dr. Giulio Santori, g.santori@ed.ac.uk, The University of Edinburgh, School of Engineering, Institute for Materials and Processes, Sanderson Building, The King's Buildings, Robert Stevenson Road, Edinburgh, Scotland, EH9 3FB, UK

Author Contributions

The manuscript was written through contributions of all authors. All authors have given approval to the final version of the manuscript. All the authors have contributed to writing the manuscript. Dr. Giulio Santori is the leader and originator of the research, Dr. Ahmed Askalany has prepared the materials, measured and regressed the isotherms, Dr. Christopher Olkis has tested the material on the desalinator, Dr. Angelo Freni, Dr. Emilia Bramanti and Mr. Dmitry Lipshin and have performed FTIR and TG measurements and interpreted the results. Dr. Luigi Calabrese and Prof. Edoardo Proverbio have performed SEM measurements.

Funding Sources

For this research Dr. Ahmed Askalany, Mr. Christopher Olkis and Dr. Giulio Santori have received funding from the EPSRC “Micro-scale energy storage for super-efficient wet appliances” project EP/P010954/1. All the remaining authors have contributed to the research supported by their home institutions.

REFERENCES

(1) Erdős, M.; de Lange, M. F.; Kapteijn, F.; Moultos, O. A.; Vlugt, T. J. H. In Silico Screening of Metal–Organic Frameworks for Adsorption-Driven Heat Pumps and Chillers. *ACS Appl. Mater. Interfaces* **2018**, *10* (32), 27074–27087. https://doi.org/10.1021/acsami.8b09343.

(2) Henninger, S. K.; Habib, H. A.; Janiak, C. MOFs as Adsorbents for Low Temperature Heating and Cooling Applications. *J. Am. Chem. Soc.* **2009**, *131* (8), 2776–2777. https://doi.org/10.1021/ja808444z.

(3) Lior, N. *Advances in Water Desalination*; Wiley, 2012.

(4) Kim, H.; Rao, S. R.; Kapustin, E. A.; Zhao, L.; Yang, S.; Yaghi, O. M.; Wang, E. N. Adsorption-Based Atmospheric Water Harvesting Device for Arid Climates. *Nat. Commun.* **2018**, *9* (1), 1191. https://doi.org/10.1038/s41467-018-03162-7.

(5) Olkis, C.; Santori, G.; Brandani, S. An Adsorption Reverse Electrodialysis System for the Generation of Electricity from Low-Grade Heat. *Appl. Energy* **2018**, *231*, 222–234. https://doi.org/10.1016/J.APENERGY.2018.09.112.

(6) Li, A.; Dong, C.; Dong, W.; Atinafu, D. G.; Gao, H.; Chen, X.; Wang, G. Hierarchical 3D Reduced Graphene Porous-Carbon-Based PCMs for Superior Thermal Energy Storage Performance. *ACS Appl. Mater. Interfaces* **2018**, *10* (38), 32093–32101. https://doi.org/10.1021/acsami.8b09541.

(7) Santori, G.; Di Santis, C. Optimal Fluids for Adsorptive Cooling and Heating. *Sustain. Mater. Technol.* **2017**, *12*. https://doi.org/10.1016/j.susmat.2017.04.005.

(8) Zaragoza, G.; Ruiz-Aguirre, A.; Guillén-Burrieza, E. Efficiency in the Use of Solar Thermal Energy of Small Membrane Desalination Systems for Decentralized Water Production. *Appl. Energy* **2014**, *130*, 491–499. https://doi.org/10.1016/J.APENERGY.2014.02.024.

(9) Dow, N.; Gray, S.; Li, J.; Zhang, J.; Ostarcevic, E.; Liubinas, A.; Atherton, P.; Roeszler, G.; Gibbs, A.; Duke, M. Pilot Trial of Membrane Distillation Driven by Low Grade Waste Heat: Membrane Fouling and Energy Assessment. *Desalination* **2016**, *391*, 30–42. https://doi.org/10.1016/J.DESAL.2016.01.023.

(10) Gao, L.; Zhang, J.; Gray, S.; Li, J.-D. Experimental Study of Hollow Fiber Permeate Gap Membrane Distillation and Its Performance Comparison with DCMD and SGMD. *Sep. Purif. Technol.* **2017**, *188*, 11–23. https://doi.org/10.1016/J.SEPPUR.2017.07.009.

(11) Bouguecha, S. T.; Aly, S. E.; Al-Beirutty, M. H.; Hamdi, M. M.; Boubakri, A. Solar Driven DCMD: Performance Evaluation and Thermal Energy Efficiency. *Chem. Eng. Res. Des.* **2015**, *100*, 331–340. https://doi.org/10.1016/J.CHERD.2015.05.044.

(12) Wang, Y.; Xu, Z.; Lior, N.; Zeng, H. An Experimental Study of Solar Thermal Vacuum Membrane Distillation Desalination. *Desalin. Water Treat.* **2014**, 1–11. https://doi.org/10.1080/19443994.2014.927187.

(13) Ng, K. C.; Thu, K.; Kim, Y.; Chakraborty, A.; Amy, G. Adsorption Desalination: An Emerging Low-Cost Thermal Desalination Method. *Desalination* **2013**, *308*, 161–179. https://doi.org/10.1016/J.DESAL.2012.07.030.

(14) Thu, K.; Yanagi, H.; Saha, B. B.; Ng, K. C. Performance Investigation on a 4-Bed Adsorption Desalination Cycle with Internal Heat Recovery Scheme. *Desalination* **2017**, *402*, 88–96. https://doi.org/10.1016/J.DESAL.2016.09.027.

(15) Freni, A.; Sapienza, A.; Glaznev, I. S.; Aristov, Y. I.; Restuccia, G. Experimental Testing of a Lab-Scale Adsorption Chiller Using a Novel Selective Water Sorbent "Silica Modified by Calcium Nitrate." *Int. J. Refrig.* **2012**, *35* (3), 518–524. https://doi.org/10.1016/J.IJREFRIG.2010.05.015.

(16) Aristov, Y. I. New Family of Solid Sorbents for Adsorptive Cooling: Material Scientist Approach. *J. Eng. Thermophys.* **2007**, *16* (2), 63–72. https://doi.org/10.1134/S1810232807020026.

(17) Aristov, Y. I.; Tokarev, M. M.; Cacciola, G.; Restuccia, G. Selective Water Sorbents for Multiple Applications, 1. CaCl2 Confined in Mesopores of Silica Gel: Sorption Properties. *React. Kinet. Catal. Lett.* **1996**, *59* (2), 325–333. https://doi.org/10.1007/BF02068130.

(18) Gordeeva, L. G.; Restuccia, G.; Cacciola, G.; Aristov, Y. I. Selective Water Sorbents for Multiple Applications, 5. LiBr Confined in Mesopores of Silica Gel: Sorption Properties. *React. Kinet. Catal. Lett.* **1998**, *63* (1), 81–88. https://doi.org/10.1007/BF02475434.

(19) Thu, K.; Chakraborty, A.; Saha, B. B.; Ng, K. C. Thermo-Physical Properties of Silica Gel for Adsorption Desalination Cycle. *Appl. Therm. Eng.* **2013**, *50* (2), 1596–1602. https://doi.org/10.1016/J.APPLTHERMALENG.2011.09.038.

(20) Mrowiec-Białoń, J.; Jarzębski, A. B.; Pająk, L. Water Vapor Adsorption on the SiO2-CaCl2sol-Gel Composites. *Langmuir* **1999**, *15* (19), 6505–6509. https://doi.org/10.1021/la990231n.

(21) Ristić, A.; Logar, N. Z.; Henninger, S. K.; Kaučič, V. The Performance of Small-Pore Microporous Aluminophosphates in Low-Temperature Solar Energy Storage: The Structure-Property Relationship. *Adv. Funct. Mater.* **2012**, *22* (9), 1952–1957. https://doi.org/10.1002/adfm.201102734.

(22) Cadiau, A.; Lee, J. S.; Damasceno Borges, D.; Fabry, P.; Devic, T.; Wharmby, M. T.; Martineau, C.; Foucher, D.; Taulelle, F.; Jun, C.-H.; et al. Design of Hydrophilic Metal Organic Framework Water Adsorbents for Heat Reallocation. *Adv. Mater.* **2015**, *27* (32), 4775–4780. https://doi.org/10.1002/adma.201502418.

(23) Youssef, P. G.; Mahmoud, S. M.; AL-Dadah, R. K. Performance Analysis of Four Bed Adsorption Water Desalination/Refrigeration System, Comparison of AQSOA-Z02 to Silica-Gel. *Desalination* **2015**, *375*, 100–107. https://doi.org/10.1016/J.DESAL.2015.08.002.

(24) Elsayed, E.; AL-Dadah, R.; Mahmoud, S.; Anderson, P. A.; Elsayed, A.; Youssef, P. G. CPO-27(Ni), Aluminium Fumarate and MIL-101(Cr) MOF Materials for Adsorption Water Desalination. *Desalination* **2017**, *406*, 25–36. https://doi.org/10.1016/J.DESAL.2016.07.030.

(25) Boman, D. B.; Hoysall, D. C.; Staedter, M. A.; Goyal, A.; Ponkala, M. J.; Garimella, S. A Method for Comparison of Absorption Heat Pump Working Pairs. *Int. J. Refrig.* **2017**, *77*, 149–175. https://doi.org/10.1016/j.ijrefrig.2017.02.023.

(26) Askalany, A. A.; Freni, A.; Santori, G. Supported Ionic Liquid Water Sorbent for High Throughput Desalination and Drying. *Desalination* **2019**, *452*, 258–264. https://doi.org/10.1016/J.DESAL.2018.11.002.

(27) Lenk, T. J.; Ratner, B. D.; Gendreau, R. M.; Chittur, K. K. IR Spectral Changes of Bovine Serum Albumin upon Surface Adsorption. *J. Biomed. Mater. Res.* **1989**, *23* (6), 549–569. https://doi.org/10.1002/jbm.820230603.

(28) Kato, K.; Tanaka, S.; Matsui, T. Quantitative Estimation of α-Helix Coil Content in Bovine Serum Albumin by Fourier Transform-Infrared Spectroscopy. *Appl. Spectrosc.* **1987**, *41* (5), 861–865.

(29) Bramanti, E.; Lenci, F.; Sgarbossa, A. Effects of Hypericin on the Structure and Aggregation Properties of β-Amyloid Peptides. *Eur. Biophys. J.* **2010**, *39* (11), 1493–1501. https://doi.org/10.1007/s00249-010-0607-x.

(30) Olkis, C.; Brandani, S.; Santori, G. A Small-Scale Adsorption Desalinator. *Energy Procedia* **2019**, *158*, 1425–1430. https://doi.org/10.1016/J.EGYPRO.2019.01.345.

(31) Olkis, C.; Brandani, S.; Santori, G. Design and Experimental Study on a Small Scale Adsorption Desalinator. *Appl. Energy* **2019**.

(32) Hussain, T.; Waters, L. J.; Parkes, G. M. B.; Shahzad, Y. Microwave Processed Solid Dispersions for Enhanced Dissolution of Gemfibrozil Using Non-Ordered Mesoporous Silica. *Colloids Surfaces A Physicochem. Eng. Asp.* **2017**, *520*, 428–435. https://doi.org/10.1016/J.COLSURFA.2017.02.007.

(33) Waters, L. J.; Hanrahan, J. P.; Tobin, J. M.; Finch, C. V.; Parkes, G. M. B.; Ahmad, S. A.; Mohammad, F.; Saleem, M. Enhancing the Dissolution of Phenylbutazone Using Syloid® Based Mesoporous Silicas for Oral Equine Applications. *J. Pharm. Anal.* **2018**, *8* (3), 181–186. https://doi.org/10.1016/J.JPHA.2018.01.004.

(34) Hespeler, D.; Kaltenbach, J.; Pyo, S. M. Glabridin SmartPearls – Silica Selection, Production, Amorphous Stability and Enhanced Solubility. *Int. J. Pharm.* **2019**, *561*, 228–235. https://doi.org/10.1016/J.IJPHARM.2019.02.028.

(35) Hussain, T. The Application of Microwave Formulation and Isothermal Titration Calorimetry for Pharmaceutical Compounds, The University of Huddersfield, 2014.

(36) Weerapol, Y.; Limmatvapirat, S.; Jansakul, C.; Takeuchi, H.; Sriamornsak, P. Enhanced Dissolution and Oral Bioavailability of Nifedipine by Spontaneous Emulsifying Powders: Effect of Solid Carriers and Dietary State. *Eur. J. Pharm. Biopharm.* **2015**, *91*, 25–34. https://doi.org/10.1016/J.EJPB.2015.01.011.

(37) Römich, C.; Merkel, N. C.; Valbonesi, A.; Schaber, K.; Sauer, S.; Schubert, T. J. S. Thermodynamic Properties of Binary Mixtures of Water and Room-Temperature Ionic

Liquids: Vapor Pressures, Heat Capacities, Densities, and Viscosities of Water + 1-Ethyl-3-Methylimidazolium Acetate and Water + Diethylmethylammonium Methane Sulfonate. *J. Chem. Eng. Data* **2012**, *57* (8), 2258–2264. https://doi.org/10.1021/je300132e.

(38) Merkel, N.; Weber, C.; Faust, M.; Schaber, K. Influence of Anion and Cation on the Vapor Pressure of Binary Mixtures of Water + Ionic Liquid and on the Thermal Stability of the Ionic Liquid. *Fluid Phase Equilib.* **2015**, *394*, 29–37. https://doi.org/10.1016/J.FLUID.2015.03.001.

(39) Krannich, M.; Heym, F.; Jess, A. Characterization of Six Hygroscopic Ionic Liquids with Regard to Their Suitability for Gas Dehydration: Density, Viscosity, Thermal and Oxidative Stability, Vapor Pressure, Diffusion Coefficient, and Activity Coefficient of Water. *J. Chem. Eng. Data* **2016**. https://doi.org/10.1021/acs.jced.5b00806.

(40) Fehrmann, R.; Riisager, A.; Haumann, M. *Supported Ionic Liquids : Fundamentals and Applications*.

(41) Perkin, S.; Crowhurst, L.; Niedermeyer, H.; Welton, T.; Smith, A. M.; Gosvami, N. N. Self-Assembly in the Electrical Double Layer of Ionic Liquids. *Chem. Commun.* **2011**, *47* (23), 6572. https://doi.org/10.1039/c1cc11322d.

(42) Henderson, Z.; Walton, A. S.; Thomas, A. G.; Syres, K. L. Water-Induced Reordering in Ultrathin Ionic Liquid Films. *J. Phys. Condens. Matter* **2018**, *30* (33), 334003. https://doi.org/10.1088/1361-648X/aad24f.

(43) Al-Oweini, R.; El-Rassy, H. Synthesis and Characterization by FTIR Spectroscopy of Silica Aerogels Prepared Using Several Si(OR)4 and R″Si(OR′)3 Precursors. *J. Mol. Struct.* **2009**, *919* (1–3), 140–145. https://doi.org/10.1016/J.MOLSTRUC.2008.08.025.

(44) Dhumal, N. R.; Kim, H. J.; Kiefer, J. Molecular Interactions in 1-Ethyl-3-

Methylimidazolium Acetate Ion Pair: A Density Functional Study. *J. Phys. Chem. A* **2009**, *113* (38), 10397–10404. https://doi.org/10.1021/jp907394v.

(45) Jeon, Y.; Sung, J.; Seo, C.; Lim, H.; Cheong, H.; Kang, M.; Moon, B.; Ouchi, Y.; Kim, D. Structures of Ionic Liquids with Different Anions Studied by Infrared Vibration Spectroscopy. *J. Phys. Chem. B* **2008**, *112* (15), 4735–4740. https://doi.org/10.1021/JP7120752.

(46) Guyomard-Lack, A.; Buchtová, N.; Humbert, B.; Le Bideau, J. Ion Segregation in an Ionic Liquid Confined within Chitosan Based Chemical Ionogels. *Phys. Chem. Chem. Phys.* **2015**, *17* (37), 23947–23951. https://doi.org/10.1039/C5CP04198H.

(47) Aristov, Y. Concept of Adsorbent Optimal for Adsorptive Cooling/Heating. *Appl. Therm. Eng.* **2014**, *72* (2), 166–175. https://doi.org/10.1016/J.APPLTHERMALENG.2014.04.077.

(48) Di Nicola, G.; Pacetti, M.; Polonara, F.; Santori, G.; Stryjek, R. Development and Optimization of a Method for Analyzing Biodiesel Mixtures with Non-Aqueous Reversed Phase Liquid Chromatography. *J. Chromatogr. A* **2008**, *1190* (1–2). https://doi.org/10.1016/j.chroma.2008.02.085.

(49) Askalany, A. A.; Saha, B. B. Derivation of Isosteric Heat of Adsorption for Non-Ideal Gases. *Int. J. Heat Mass Transf.* **2015**, *89*, 186–192. https://doi.org/10.1016/J.IJHEATMASSTRANSFER.2015.05.018.

(50) Srinivasan, K.; Saha, B. B.; Ng, K. C.; Dutta, P.; Prasad, M. A Method for the Calculation of the Adsorbed Phase Volume and Pseudo-Saturation Pressure from Adsorption Isotherm Data on Activated Carbon. *Phys. Chem. Chem. Phys.* **2011**, *13* (27), 12559. https://doi.org/10.1039/c1cp20383e.

(51) Sapienza, A.; Velte, A.; Girnik, I.; Frazzica, A.; Füldner, G.; Schnabel, L.; Aristov, Y.

"Water - Silica Siogel" Working Pair for Adsorption Chillers: Adsorption Equilibrium and Dynamics. *Renew. Energy* **2017**, *110*, 40–46. https://doi.org/10.1016/J.RENENE.2016.09.065.

(52) Olkis, C.; Brandani, S.; Santori, G. Cycle and Performance Analysis of a Small-Scale Adsorption Heat Transformer for Desalination and Cooling Applications. *Chem. Eng. J.* **2019**, *378*, 122104. https://doi.org/10.1016/j.cej.2019.122104.

(53) Thu, K.; Ng, K. C.; Saha, B. B.; Chakraborty, A.; Koyama, S. Operational Strategy of Adsorption Desalination Systems. *Int. J. Heat Mass Transf.* **2009**, *52* (7–8), 1811–1816. https://doi.org/10.1016/J.IJHEATMASSTRANSFER.2008.10.012.